

## Thermal decomposition of calcium citrate tetrahydrate

Seham A.A. Mansour

*Chemistry Department, Faculty of Science, Minia University, El-Minia (Egypt)*

(Received 19 May 1993; accepted 14 June 1993)

### Abstract

The thermal decomposition of calcium citrate tetrahydrate in dynamic air or dry nitrogen has been studied thoroughly. Thermal events encountered throughout the decomposition range (room temperature to 1000°C) have been monitored by TG, DTA and DSC. The encountered events have been characterized by analysing the decomposition solid products using X-ray diffractometry, IR spectroscopy and scanning electron microscopy (SEM). Non-isothermal kinetic and thermodynamic parameters ( $A$ ,  $k$ ,  $\Delta E$ ,  $\Delta H$ ,  $C_p$  and  $\Delta S$ ) have been determined. The results show that  $\text{Ca}_3(\text{C}_6\text{H}_5\text{O}_7)_2 \cdot 4\text{H}_2\text{O}$  dehydrates in two successive steps at 60–140°C and 140–190°C each involving release of two moles of water. The ultimate decomposition product has been found to be CaO which formed above 640°C in air or dry nitrogen flow. SEM examinations indicate the formation of fusion nuclei accompanying the second dehydration step. Decomposition pathways in air and nitrogen are proposed.

### INTRODUCTION

Metal citrates are often formed in natural systems, in various conversions and in processes of food-stuff manufacture [1–3]. Many of these processes occurring at elevated temperatures are associated with the decomposition of citric acid or the metal citrates formed.

Citric acid, which is widely used in the food industry [4, 5], is produced from glucose by fungi or yeasts [6, 7]. In its commercial manufacturing methods, an important stage is the separation of the acid in the form of precipitated calcium citrate [5, 7, 8], in the hot state; thus it is easily separable from accompanying tartrates, oxalates and malates. Hence, it is interesting to follow carefully the thermal decomposition course of such metal citrates. The present investigation focussed on the thermal behaviour of calcium citrate tetrahydrate.

## EXPERIMENTAL

### *Calcium citrate*

$\text{Ca}_3(\text{C}_6\text{H}_5\text{O}_7)_2 \cdot 4\text{H}_2\text{O}$  was a certified AR grade, BDH product. It is denoted in the text by CaCi.

### *Thermal analysis*

Thermogravimetry (TG), differential thermal analysis (DTA) and differential scanning calorimetry (DSC) were carried out using an automatically recording Shimadzu thermal analyzer model 30H, Japan. DSC curves were recorded under dynamic atmosphere of dry nitrogen ( $30 \text{ ml min}^{-1}$ ), at the heating rates  $\theta$  of 5, 10 and  $20^\circ\text{C min}^{-1}$ . TG and DTA were performed under dynamic air ( $30 \text{ ml min}^{-1}$ ) at  $\theta$  of 5, 10, 20 and  $50^\circ\text{C min}^{-1}$ .

The techniques adopted and a detailed description of the procedure and equations used to determine the non-isothermal kinetic and thermodynamic parameters have been given in a previous paper [9].

### *Product analysis*

In view of the thermal analysis results (*vide infra*), CaCi was decomposed by calcining in still air atmosphere ( $230\text{--}900^\circ\text{C}$ ) for 2 h. The solid products were examined by IR spectroscopy, X-ray diffractometry (XRD) and scanning electron microscopy (SEM).

IR spectra were obtained at a resolution of  $5.3 \text{ cm}^{-1}$ , over the frequency range  $4000\text{--}250 \text{ cm}^{-1}$ , by means of a model 580B Perkin-Elmer double-beam spectrophotometer (UK). The spectra were taken from thin ( $\leq 20 \text{ mg cm}^{-1}$ ) KBr discs containing less than 1% by mass of the test samples.

XRD powder diffractograms were obtained using a model JS X-60 PA Jeol diffractometer (Japan), with a source of Ni-filtered Cu  $K\alpha$  radiation ( $\lambda = 1.542 \text{ \AA}$ ). The diffraction patterns ( $I/I_0$  versus d-spacing ( $\text{\AA}$ )) determined therefrom were compared with the relevant ASTM standards [10].

Microscopic examinations were made using a Jeol 35 CF scanning electron microscope. Samples of CaCi and its decomposition products were mounted on the support by clear adhesive and coated with an Au/Pd layer

to render charging effects. The photographs presented here illustrate typical and reproducible structures that are considered to be significant.

## RESULTS AND DISCUSSION

TG and DTA curves for CaCi at  $10^{\circ}\text{C min}^{-1}$ , in a dynamic atmosphere of air or nitrogen, are shown in Fig. 1. The curves indicate that CaCi decomposes in air via five thermal events occurring at 60–140 (I), 140–190 (II), about 230 (III), 340–480 (IV) and 640–780°C (V). All of these events are mass loss processes except event III which is mass invariant.

### *Characterization of the thermal events*

#### *Events I and II*

Figure 1 indicates that in air events I and II are two successive endothermic processes, maximized at 85°C and 145°C respectively and each was accompanied by 6.3% loss of the original mass. Such mass loss equals that expected for the release of two moles of water from CaCi



The IR spectrum of the calcination product at 230°C (Fig. 2) displays all the characteristic bands of citrate [11] and shows an obvious lack of the absorption band of water around  $3440\text{ cm}^{-1}$ .

The effect of heating rate on the thermal behaviour of CaCi in air is shown in Fig. 3. The shifts of temperature at which events I–IV are maximized, were used to estimate the kinetic parameters compiled in Table 1. The results obtained indicate that the activation energy  $\Delta E$  associated with the second dehydration process ( $90\text{ kJ mol}^{-1}$ ) is slightly higher than that corresponding to the first one ( $77\text{ kJ mol}^{-1}$ ; see Table 1). This may infer the presence of some difficulty accompanying the release of the second two moles of water and/or participation of another physical process, e.g. commencement of melting.

Under dynamic nitrogen atmosphere, these two dehydration processes also occurred endothermically (Fig. 1) as did their responses towards DSC measurements (Fig. 4). The associated activation energies  $\Delta E$  of 69 and  $61.9\text{ kJ mol}^{-1}$  agree well with the reported values [5, 7]. Moreover, the enthalpic change  $\Delta H$  and the entropic change  $\Delta S$  were found to be higher for event II than that for event I (Table 2), which indicates an increase in

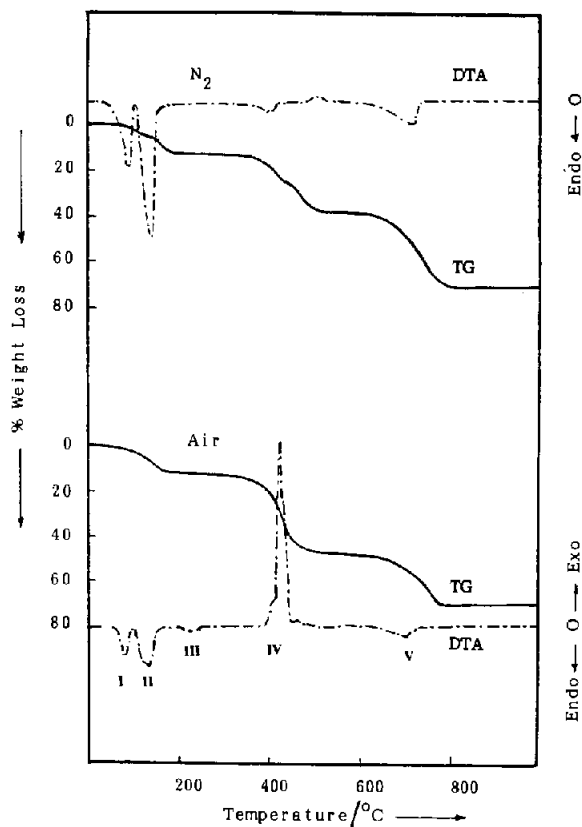


Fig. 1. TG and DTA curves for CaCi at  $\theta = 10^\circ\text{C min}^{-1}$  in dynamic ( $30\text{ ml min}^{-1}$ ) atmosphere of air or dry nitrogen.

the disorder accompanying the complete removal of water of crystallization.

### Event III

The DTA curve given in Fig. 1 shows event III as a very small mass-invariant endothermic process maximized at  $230^\circ\text{C}$ . This process is most probably attributed to melting of CaCi [5], associated with an activation energy  $\Delta E$  of  $165.5\text{ kJ mol}^{-1}$  (Table 1).

### Event IV

Figure 1 reveals that event IV proceeds exothermically in air in the temperature range  $340\text{--}480^\circ\text{C}$ . The shape of both the TG and DTA features corresponding to this event indicate the complexity of the processes involved. The decomposition solid product of CaCi at  $600^\circ\text{C}$

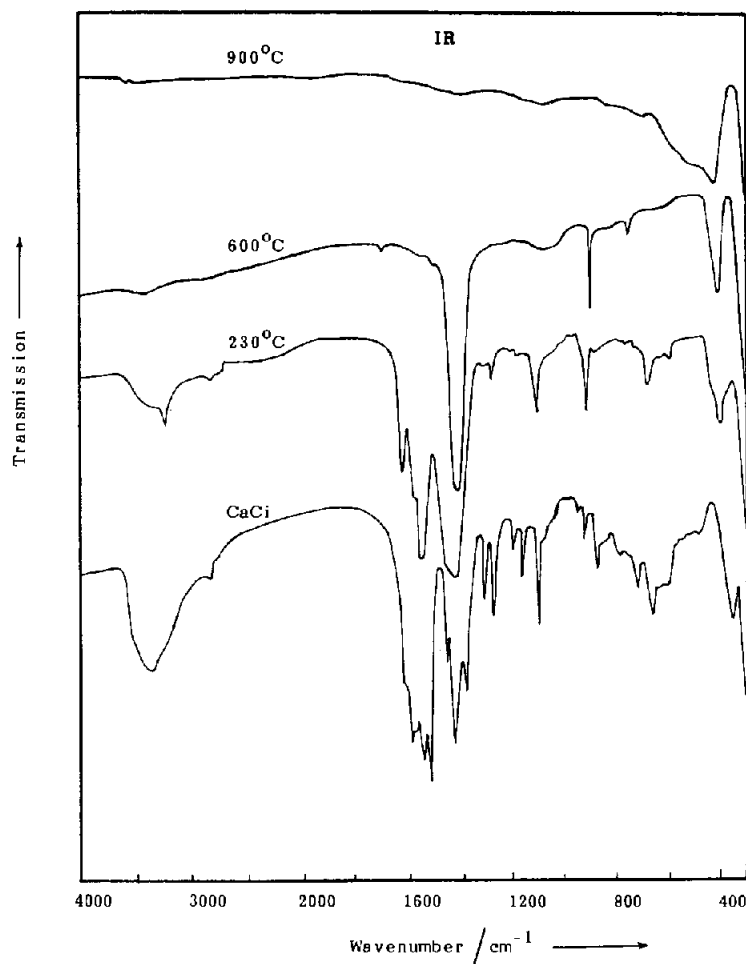
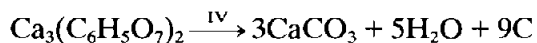


Fig. 2. IR spectra of CaCi and its calculation products at the temperatures indicated.

displays an IR spectrum (Fig. 2) of CaCO<sub>3</sub> (calcite structure) [12]. XRD of this decomposition product (Fig. 5) exhibits the characteristic lines of CaCO<sub>3</sub> (ASTM card no. 5–586), while those for the original CaCi (ASTM card no. 28–2003) have disappeared. These results, together with the observed mass loss of 47% suggest that event IV involves the transformation of anhydrous calcium citrate to calcium carbonate



The carbon formed from this event would not naturally stay in the elemental form at such a high temperature (above 340°C) particularly in the presence of atmospheric oxygen. Therefore, it must have been turned into CO and/or CO<sub>2</sub>.

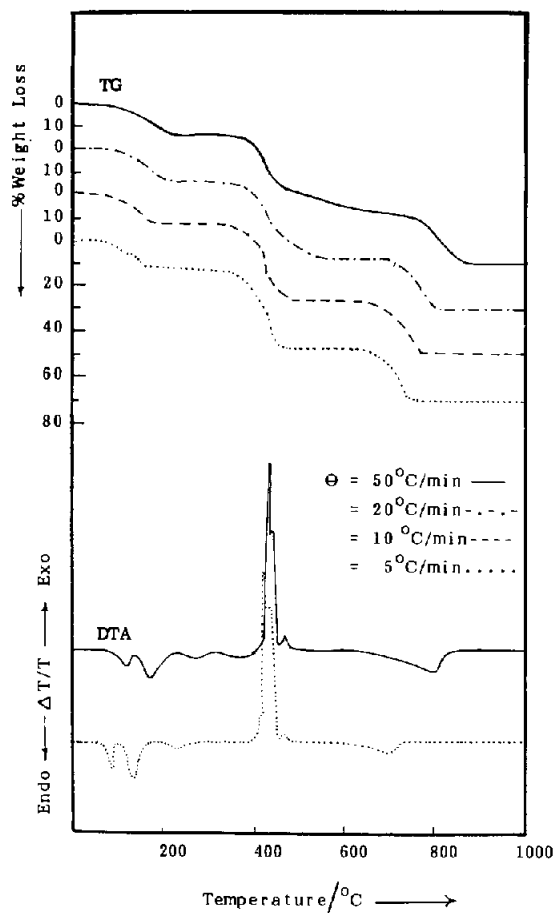


Fig. 3. TG and DTA curves recorded for CaCl<sub>2</sub> at the heating rates  $\theta$  indicated in a dynamic (30 ml min<sup>-1</sup>) atmosphere of air.

TABLE 1

Non-isothermal kinetic parameters of the thermal events occurring throughout the decomposition course of CaCl<sub>2</sub> in air<sup>a</sup>

Event	$k/\text{min}^{-1}$	$\log A$	$\Delta E/\text{kJ mol}^{-1}$	$\Delta T/T$
I	$2.3 \times 10^{-1}$	10	77	endo
II	$3.0 \times 10^{-1}$	10	90	endo
III			165	endo
IV	$8.0 \times 10^{-1}$	16	400	exo
V	$2.0 \times 10^{-1}$	8	180	endo

<sup>a</sup> Kinetic parameters for thermal events I, II, IV and V were calculated from TG data, whereas for event III DTA data were used.

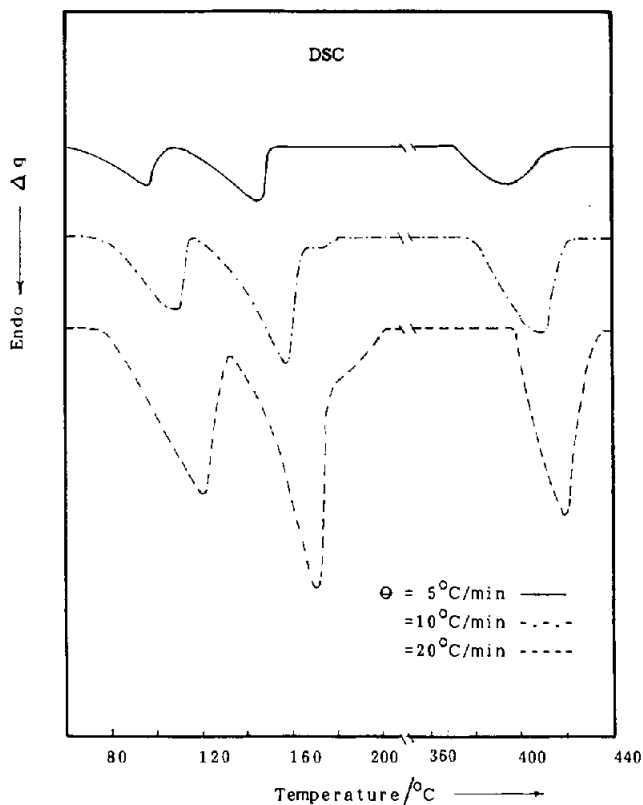


Fig. 4. DSC curves recorded for CaCi at the heating rates  $\theta$  indicated in a dynamic ( $30 \text{ ml min}^{-1}$ ) atmosphere of dry nitrogen.

Earlier studies [5, 11] reported that the decomposition of calcium citrate into calcium carbonate involves the formation of calcium aconitate ( $\text{Ca}_3(\text{C}_6\text{H}_3\text{O}_6)_2$ ) as intermediate. However, in the present investigation, such a compound has not been isolated even at the slowest heating rate used ( $5^\circ\text{C min}^{-1}$ ). However, calcium aconitate may have been formed and instantaneously decomposed, which may be the reason for the decompose

TABLE 2

Non-isothermal kinetic and thermodynamic parameters of the thermal events occurring throughout the decomposition course of CaCi up to  $450^\circ\text{C}$  in dry  $\text{N}_2$  atmosphere, calculated from DSC curves

Event	$\Delta E/\text{kJ mol}^{-1}$	$\ln A$	$k/\text{min}^{-1}$	$\Delta H/\text{kJ mol}^{-1}$	$G_p/\text{J g}^{-1}$	$\Delta S(\text{J K}^{-1} \text{g}^{-1})$	$\Delta q/q$
I	69	21	0.57	87.3	2.16	0.40	endo
II	69.9	16	0.40	126.1	3.20	0.50	endo
III	196.6	33	0.50	105.2	3.40	0.15	endo

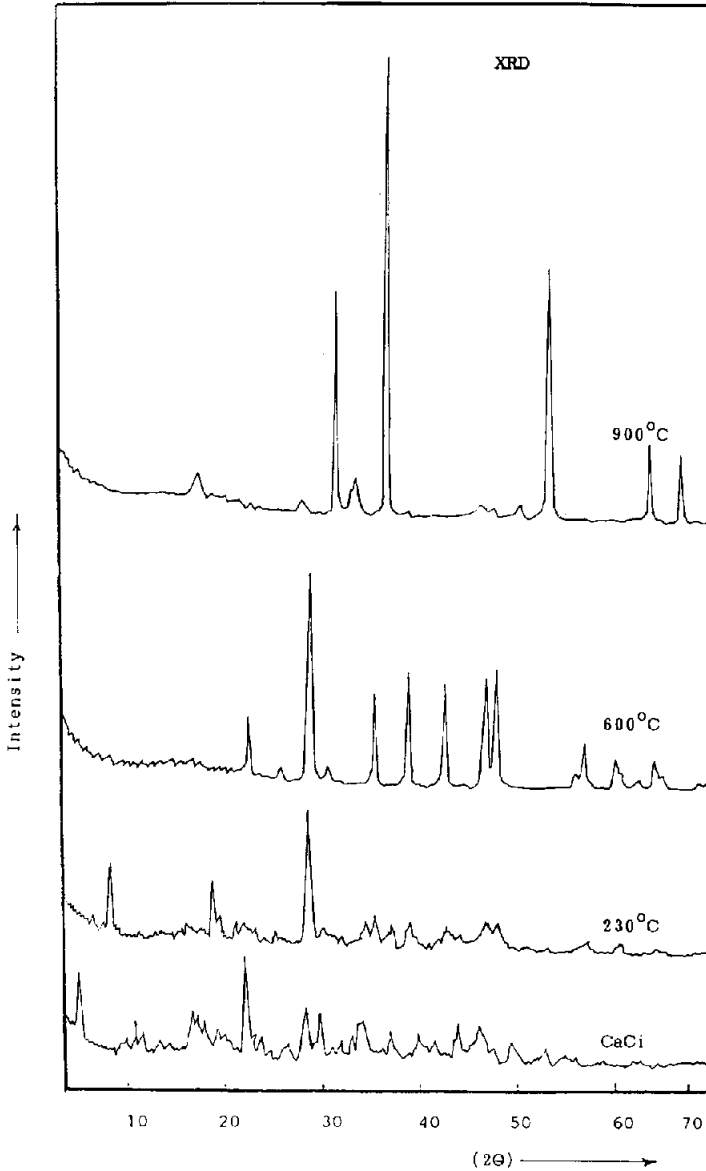


Fig. 5. XRD powder diffractograms for CaCi and its calcination products at the temperatures indicated.

shape of the DTA curve for this event as well as the appearance of more than one slope in the TG curve (Figs. 1 and 3).

Figure 1 indicates that event IV occurred endothermically under dynamic nitrogen atmosphere, in the temperature range 370–530°C. The associated mass loss amounts to 25.5% bringing the total loss up to 38% of the original mass. Such a mass loss is fairly close to that calculated (37.9%)

for the occurrence of the reaction

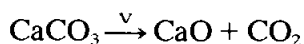


It is worth mentioning here that this event commenced exothermically under dynamic atmosphere of air (Figs. 1 and 3). The reason for the appearance of such an exotherm must be the occurrence of pyrolysis of the carbon formed in this event by atmospheric oxygen to give CO and/or CO<sub>2</sub>. Such pyrolysis does not naturally occur in nitrogen flow; hence this event proceeds endothermically under such conditions. This event also responded towards DSC measurement endothermically, with an associated activation energy  $\Delta E$  of 196 kJ mol<sup>-1</sup> (Table 2). Both  $\Delta S$  and  $\Delta H$  values (Table 2) were found to be low, suggesting a decrease in disorder for this event.

#### *Event V*

The thermal decomposition course of CaCi in air or nitrogen flow ends up with event V occurring endothermically in the temperature range 640–780°C in both atmospheres. The corresponding mass loss accompanying this event amounts to 22% in dynamic air and 32% in nitrogen flow bringing the total loss up to 70% in both cases. Such mass loss is very close to that calculated (70.5%) for the transformation of CaCi into CaO. The IR spectrum (Fig. 2) of the calcination product at 900°C in still air displays the characteristic bands of CaO [13]. This product shows an X-ray diffractogram (Fig. 5) which matches well with CaO (ASTM card no. 4-777). The activation energy ( $\Delta E$ ) associated with this event in air was found to be 180 kJ mol<sup>-1</sup> (Table 1). Hence, event V would involve the reactions

(i) in air



(ii) in nitrogen



#### *Electron microscopy*

The morphological changes accompanying the thermal decomposition of CaCi were followed up by SEM examination of samples of the parent salt as well as of the decomposition products used in the IR and XRD work. SEM of the parent CaCi showed that the salt was composed of irregular aggregates of plate-like crystallites. A typical assemblage is shown in Fig. 6(a). Dimensions of the crystallites varied appreciably and their shapes were often irregular (Fig. 6(b)). Examination of the product from thermal events I and II (i.e. the calcination product at 230°C), revealed the

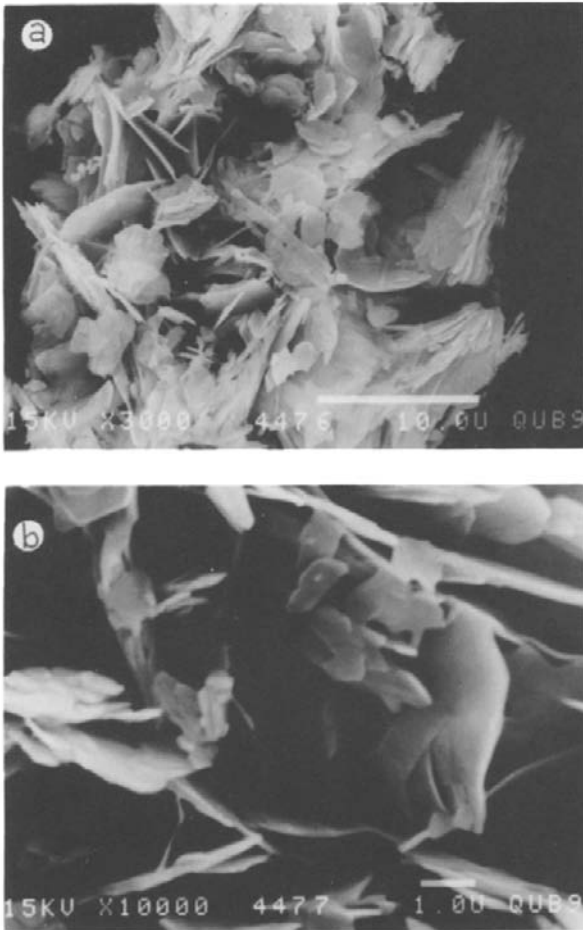


Fig. 6. Scanning electron micrographs of the parent  $\text{CaCl}_2$  showing (a) an assemblage of plate-like crystallites of (b) variable dimensions and irregular shapes.

generation of rounded local assemblages of froth-like material. Characteristic features of these assemblages are illustrated in the SEM in Fig. 7 (a, b). These structures were apparently generated underneath the crystallite surfaces. Hence, it could be suggested that events I and II were accompanied by or ended up with formation of zones of local melting, which are usually referred to as “fusion nuclei” [14], customarily generated at internal pores or other zones of crystal imperfection. Since the parent salt crystallites had smooth surfaces (Figs. 6(a, b)), these fusion nuclei would most probably be generated at crystal imperfections. A typical fusion nucleus is shown in the right side of the upper part of Fig. 7(a). An undamaged spherical particle is seen in the lowest right of this nucleus, while in its middle, broken-open spheres are clear revealing the froth-like internal structure which is seen in greater detail in Fig. 7(b).

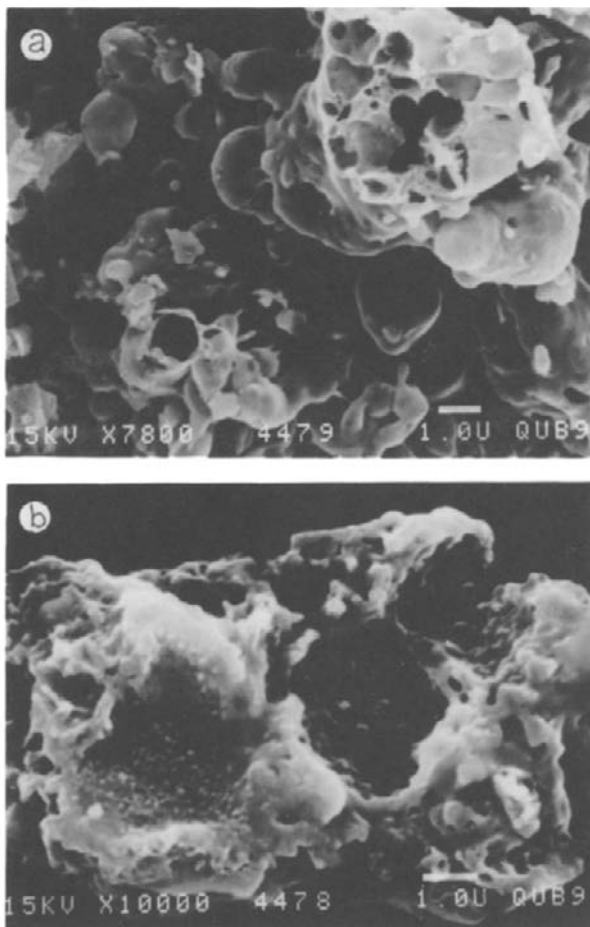


Fig. 7. Scanning electron micrographs of the calcination product at 230°C revealing the generation of (a) fusion nuclei and (b) a froth-like internal structure.

Scanning electron micrographs of the calcination product at 600°C, which was found from the reported results and discussion to be an XRD verified  $\text{CaCO}_3$ , revealed evidence of its formation from the molten phase. The material showed a foam-like structure, containing irregular and shapeless pores of various sizes (Fig. 8(a)). Raising the calcination temperature to 800°C resulted in marked morphological changes. The SEM of this product revealed the formation of an entirely new crystalline structure (Fig. 8(b)) of the CaO produced. However, a small residue of the foam-like structure of  $\text{CaCO}_3$  is visible. The micrograph of the calcination product at 900°C (Fig. 8(c)), i.e. after complete decomposition, showed aggregation of the CaO crystallites formed.

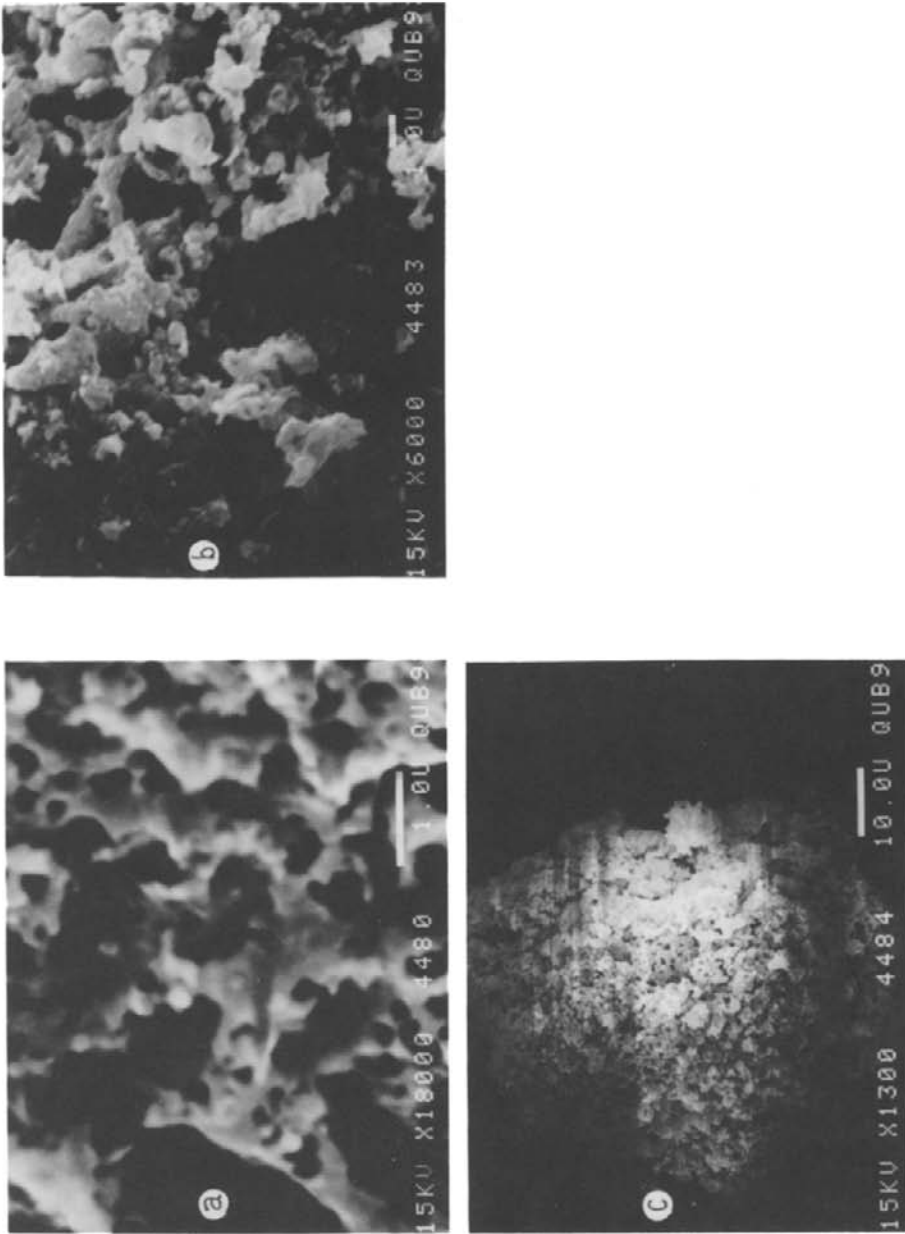
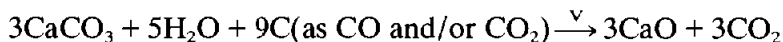
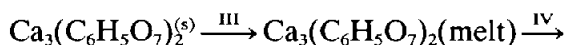
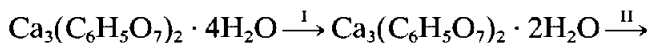


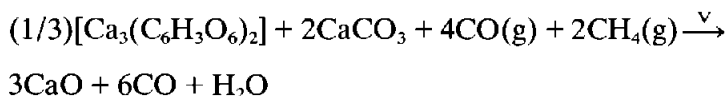
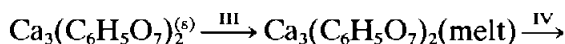
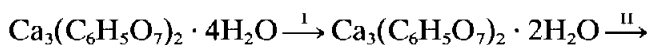
Fig. 8. Scanning electron micrographs of the calcination product at 600°C, showing (a) foam-like structure, (b) the calcination product at 800°C, showing the formation of new crystalline structure, and (c) the calcination product at 900°C.

## CONCLUSIONS

(1) The thermal decomposition of CaCi in air flow involves the following pathways



(2) In dry nitrogen flow the following pathways may be involved



The Roman numerals indicate the associated thermal events.

(3) SEM observations indicated the formation of zones of local melting (“fusion nuclei”) during the dehydration process.

## ACKNOWLEDGEMENTS

It is a pleasure to thank the Queen’s University of Belfast, particularly the staff of the electron microscope for assistance in obtaining the electron micrographs. Thanks are also due to the Egyptian Government for the grant of a fellowship.

## REFERENCES

- 1 The Calendar of Food Chemistry, WPL is, Warszawa, 1954.
- 2 Z. Ilczuk, *The Progress of Microbiology*, Part IV, PWN, Warszawa, 1966.
- 3 J. Janicek, J. Pokorny and J. Dawidek, *Food Chemistry*, WNT, Warszawa, 1977.
- 4 J. Mastowska, J. Baranowski, E. Chruscinska, A. Baranowska and K. Marszal, *Zesz. Nauk. Politech. Lodz., Technol. Food Chem.*, 36 (1980) 321.
- 5 J. Mastowska, *J. Therm. Anal.*, 29 (1984) 896.
- 6 List Pure Kulture of Microorganisms, Department of Food Chemistry, Technical University of Lodz, Lodz, 1979.
- 7 J. Mastowska, M. Bielawski and A. Baranowska, *Thermochim. Acta*, 92 (1985) 235.
- 8 J. Supniewski, *Inorganic Synthesis*, PWN, Warsaw, 1958.

- 9 S.A.A. Mansour, *Thermochim. Acta*, 228 (1993) 155.
- 10 W. Frank et al. (Eds.), *Powder Diffraction File for Inorganic Phase*, Int. Center for Diffraction Data Philadelphia, PA, 1981.
- 11 A. Srivastava, V.G. Gunjikar and A.P.B. Sinha, *Thermochim. Acta*, 117 (1987) 201.
- 12 S.D. Ross, *Inorganic Infrared and Raman Spectra*, McGraw-Hill, Maidenhead, UK, 1972, p. 144.
- 13 F.F. Bentley, L.D. Smithson and A.L. Rozek, *Infrared Spectra and Characteristic Frequencies  $\approx 700\text{--}300\text{ cm}^{-1}$* , Wiley, New York, 1968, p. 1513.
- 14 A.K. Galwey, *Proc. 7th Int. Conf. Therm. Anal.*, Wiley, New York, 1982, p. 38.